

# LUMPED METHOD FOR CALCULATING THE OPTICAL EFFICIENCY OF RADIALLY STAGGERED HELIOSTAT FIELDS

J.E. Hoffmann

Dept. of Mechanical & Mechatronic Engineering,  
Stellenbosch University, Stellenbosch, South Africa; Phone +27 21 808 3554; E-mail ([hoffmaj@sun.ac.za](mailto:hoffmaj@sun.ac.za))

## Abstract

Central receiver plant is slowly gaining acceptance in the energy market, raising the need of for planning authorities and engineers to do quick preliminary analyses of such plant. A fast, reasonably accurate method, based on geometrical projection of a heliostat's image on its immediate neighbours, is presented to calculate the optical (cosine, blocking and shading) efficiency for a radially staggered surround heliostat field based upon a lumped geometric approach. Blocking and shading is predicted, using calculation stencils of four and seven heliostats respectively. The model was used to simulate the solar field of the Gemasolar solar power plant. The model is in reasonable agreement with limited published data during normal plant operating hours. The model is rather optimistic in predicting shading losses close to sunrise and sunset, as it neglects the shading contribution from heliostats outside the calculation stencil. However, the solar irradiation decreases as the secant of the zenith angle, reducing the overall effect of the error at large zenith angle. Expanding the shading stencil decreased the shading errors close to sunset and sunrise significantly, but at the expense of computational effort. The method should be useful for pre-feasibility studies and macro decision making, but is no replacement for detailed design tools.

*Keywords: heliostat efficiency, lumped model, image projection*

## 1. Introduction

Commercial central receiver solar power plants are slowly making an impact on the energy scene. The 20 MW<sub>e</sub> Gemasolar [1] power plant in Spain was commissioned in 2011, the 377 MW<sub>e</sub> Ivanpah [2] plant in 2013, whilst the 110 MW<sub>e</sub> Crescent Dunes [3] plant is scheduled to start producing electricity towards the end of 2014, and the 50 MW<sub>e</sub> Khi-1 [4] plant early in 2015.

The solar field of a large central receiver plant comprise of thousands of heliostats. Each heliostat's position is carefully optimized, since the heliostat field typically accounts for about 40 % of the total plant cost. Calculating the annual performance of the field, and in the extreme, optimizing the

field layout for a new plant can take days of computation. This expense is often not warranted, and the accuracy not required during preliminary planning.

Methods and tools to calculate and optimize the performance of heliostat fields abound [5 – 8]. These methods are accurate, yet computationally expensive, making them ill-suited for initial calculations. During the pre-feasibility phase of such a project, plant parameters are not yet decided, and a computationally fast method is required to evaluate different designs, as performance calculations often involves integration over a typical meteorological year. Such a method should faithfully capture physics, and be reasonably accurate. Once the design has crystallized, detailed design and performance assessment tools are required. The latter is often developed in-house by plant designers, and is not disclosed in the open literature.

Design tools typically rely on ray tracing, convolution methods or surface tessellation techniques. Hence, numerous calculations are required for each individual heliostat at any particular instance of time. Further limitations may be imposed. The CAMPO [7] code is limited to regular heliostat fields, but Luchman et al [8] has shown that these may not necessarily be optimal. Leonardi and D'Aguanno [6] indicated that field performance is dominated by zenith angle, and to a lesser degree by azimuth angle. This view is reinforced by Gauche et al [9]. Haman et al [10] calculated the projection of the four corners of a heliostat onto another to find the shading and blocking losses, whilst Gauche et al [11] considered the projection of the heliostat onto a copy of itself for the same purpose. Gauche et al [11] has shown that field performance can be predicted reasonably accurate by dividing the field into a number of computational cells, with a reference heliostat representing the average performance of all heliostats in that particular cell. In their work, they considered a square field, with an in-line heliostat lay-out on a Cartesian grid. Circular and/or irregular fields can be simulated by changing the number of heliostats represented by computational cell. This has reduced the calculation load drastically, yet their results were within 10 % of those predicted by ray tracing.

This paper expands the work of Gauche et al [11] to radially staggered fields, but also borrows ideas from Leonardi and and D'Aguanno [6] and Haman et al [10]. It presents a fast, albeit approximate method to evaluate the optical efficiency of a pre-determined heliostat field for a central receiver solar power plant. The method should be useful for pre-feasibility studies and macro decision making, but is no replacement for detailed design tools.

## 2. Model description

The method presumes a surround heliostat field, with origin at the central receiver, the  $x$ -coordinate pointing due east,  $y$  north and  $z$  up. For mathematical expedience,  $z = 0$  corresponds to the centre point of the heliostats. Some key plant parameters, such as site coordinates, number and size of heliostats is assumed to be known a priori. A regular (constant offset between heliostats in the radial and circumferential direction) radially staggered arrangement is adopted within any individual cell. All the heliostats inside the cell are lumped together and are represented by a single heliostat at the cell centre. Blocking and shading are calculated from vector algebra for a stencil of three (blocking) and six (shading) neighbouring heliostats surrounding the representative heliostat. Neighbouring heliostats have an identical spatial orientation as the representative heliostat, except for their offset in the radial and circumferential directions. Furthermore, blocking and shading calculations require accurate information about the sun's position at all times. Irregular fields can be mimicked by adjusting the number of heliostats in each lumped cell accordingly.

### 2.1 Solar angles

Solar radiation is calculated from a simple model, based upon the local solar time, and a solar year starting on the winter solstice in the Northern Hemisphere. According to Duffie and Beckman [12], the sun's zenith angle is given by

$$\theta = \cos^{-1}\{\cos\psi \cos \delta \cos \Omega + \sin \psi \sin \delta\} \quad \dots (1)$$

with  $\psi$  the latitude,  $\delta$  the sun's declination angle (here expressed in degrees)

$$\delta = -23.45 \cos\left(\frac{2\pi N}{365}\right) \quad \dots (2)$$

$N$  is the number of days since the summer solstice. The hour angle  $\Omega$  ( $\Omega = 0$  at solar noon, negative in the morning and positive in the afternoon), given by

$$\Omega = \pi\left(\frac{h}{12} - 1\right) \quad \dots (3)$$

Here,  $h$  is the local solar time. The proposed model aims to provide a fast and reasonably robust estimate of optical field

efficiency. Reasonable estimates of the solar angles, rather than direct normal irradiation (DNI) is required. Nowadays, DNI data is available for almost anywhere, but the following approximate model was adopted for its additional mathematical insights. In the absence of actual DNI data, the DNI can be approximated by

$$DNI = I_0 e^{-\alpha/\cos\theta} \quad \dots (4)$$

with  $I_0$  the solar constant. The turbidity factor  $\alpha$  is tuned to yield the correct average annual DNI for any specific site, or a similar nearby site for which the DNI is known. In essence, the model assumes cloudless skies every day of the year, but the maximum DNI is toned down to account for occasional overcast conditions. It does not take seasonal variations in the turbidity factor into account.

The sun's azimuth angle is calculated from [12]

$$\phi = \text{sign}(\Omega) \left| \cos^{-1} \left\{ \frac{\cos \theta \sin \psi - \sin \delta}{\sin \theta \cos \psi} \right\} \right| \quad \dots (5)$$

### 2.2 Heliostat Field

The field is divided into discrete zones, with a representative heliostat at the centre of each zone [11]. Each zone contains a number of heliostats identical to the representative heliostat at the centroid of the zone, as shown in figure 1. The radial and circumferential spacing of the heliostats inside each zone is kept constant, but the spacing may vary from zone to zone, as shown in figure 2. Taking advantage of the inherent circular symmetry of a surround field, sparsely populated zones, say in the south field, are treated the same as the more densely populated north field (assuming a plant in the Northern Hemisphere). A weighting function, proportional to the actual number of heliostats in the zone, is introduced to account for sparsely populated zones.

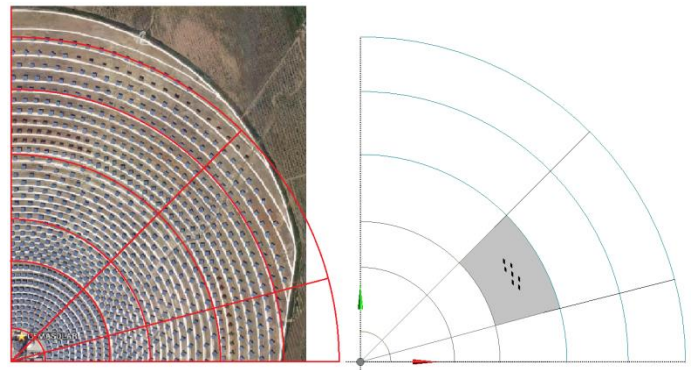


**Figure 1.** Aerial photograph of a quarter field of the Gemasolar Plant (Google Maps, [13]), and division into computational cells. Shading stencil is shown in one representative cell.

### 2.3 Cosine efficiency

The cosine efficiency depends on the heliostat orientation relative to an incoming ray from the sun, and is given by

$$\eta_{cos} = \cos\varphi \quad \dots (6)$$

with

$$\varphi = 0.5 \cos^{-1}(\vec{T} \cdot \vec{S}) \quad \dots (7)$$

with  $\vec{T}$  the unit vector pointing from the reference heliostat to the receiver, and  $\vec{S}$  the unit vector pointing at the sun. The latter is given by [12]

$$\vec{S} = \cos\phi \sin\theta \vec{i} + \sin\phi \sin\theta \vec{j} + \cos\theta \vec{k} \quad \dots (8)$$

with  $\vec{i}$ ,  $\vec{j}$  and  $\vec{k}$  unit vectors pointing in the pointing in the  $x$ - (east),  $y$ - (north) and  $z$ - (up) directions respectively.

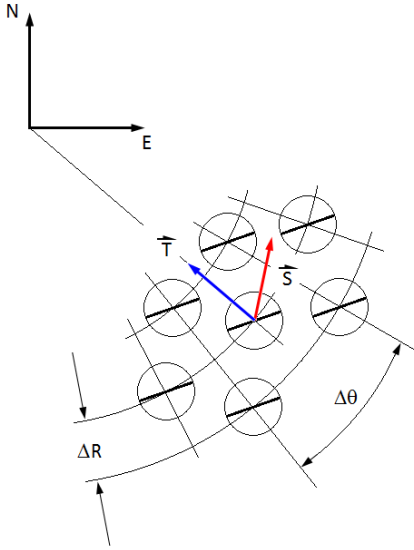


**Figure 2..** Definition sketch for radially staggered field.

### 2.4 Blocking Efficiency

Blocking is calculated on a stencil of 4 heliostats, as shown in figure 3 for a heliostat field in the Southern hemisphere. Blocking interference is calculated from solid analytic geometry, as originally proposed by Sassi [14]. Heliostat spacing within each zone is assumed to be known a priori, and is typically derived from existing heliostat fields. As a minimum, one should adhere to a spacing that would prevent interference between neighbouring heliostats, i.e.

$$R \Delta\theta > \sqrt{H^2 + W^2} \quad \dots (9)$$

and

$$\Delta R > \sqrt{H^2 + W^2} \cos\left(\frac{\Delta\theta}{2}\right) \quad \dots (10)$$

with  $H$  the height and  $W$  the width of the heliostat.

Staggered fields tend to have a high blocking efficiency, but the non-blocking condition set by Siala and Eyaleb [15] is not enforced. The latter typically results in a sparse heliostat field, especially far away from the tower. Such a field will make ill use of the available land, and suffer unnecessarily from attenuation losses. The merits of such a field are subject to optimization.

The images of heliostats 2 - 4 are projected onto a plane through the centre of heliostat 1 perpendicular to the tower vector  $\vec{T}$ . This model assumes a rectangular projection, and the distance between the projected centres of heliostats 1 and 2 in the projection plane is given by [16]

$$|\vec{P}'_{12}| = |\vec{P}_{12} - (\vec{P}_{12} \cdot \vec{T})\vec{T}| \quad \dots (11)$$

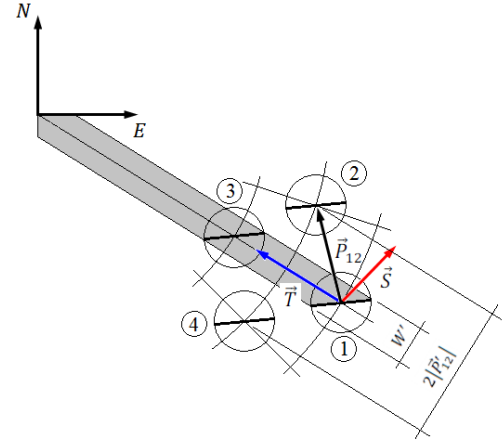


**Figure 3.** Blocking stencil for radially staggered field.

The relative position vector  $\vec{P}_{12}$  is given by

$$\vec{P}_{12} = (x_2 - x_1)\vec{i} + (y_2 - y_1)\vec{j} + (z_2 - z_1)\vec{k} \quad \dots (12)$$

The projection of  $\vec{P}_{12}$  on the plane with unit normal  $\vec{T}$  is decomposed into a vertical and horizontal component in the  $T$  plane. To find the vertical component,  $\vec{P}_{12}$  is projected onto a vertical plane containing  $\vec{T}$ . The plane normal  $\vec{n}$  of this plane is found by noting that it will also contain the vector pointing from the reference heliostat to the base of the tower,  $\vec{T}'$ .

Hence

$$\vec{n} = \frac{\vec{T} \times \vec{T}'}{|\vec{T} \times \vec{T}'|} \quad \dots (13)$$

and

$$\Delta H = |\vec{P}'_{12}| = |\vec{P}'_{12} - (\vec{P}'_{12} \cdot \vec{n})\vec{n}| \quad \dots (14)$$

The horizontal component of this projection in the  $T$  plane is found from Pythagoras' hypothesis.

$$\Delta W = \sqrt{(|\vec{P}'_{12}|)^2 - (\Delta H)^2} \quad \dots (15)$$

The projected image of the heliostat 1 on the  $T$  plane is also required. The heliostat normal vector  $\vec{h}$  is given by

$$\vec{h} = \frac{\vec{s} \cdot \vec{T}}{|\vec{s} \cdot \vec{T}|} \quad \dots (16)$$

It's projection onto a vertical plane through  $\vec{T}$  is

$$\vec{h}' = \vec{h} - (\vec{h} \cdot \vec{n})\vec{n} \dots (17)$$

Hence, the heliostat is tilted at an angle  $\beta$  relative to  $\vec{T}$  in a vertical plane, with

$$\beta = \cos^{-1} \left( \frac{\vec{T} \cdot \vec{h}'}{|\vec{T} \cdot \vec{h}'|} \right) \quad \dots (18)$$

The projected height of the heliostat onto the  $T$  plane is

$$H' = H \cos \beta \quad \dots (19)$$

To find the yaw angle, the heliostat normal is projected onto a plane with unit vector  $\vec{m}$  that is orthogonal to both  $\vec{T}$  and  $\vec{n}$

$$\vec{m} = \frac{\vec{T} \times \vec{n}}{|\vec{T} \times \vec{n}|} \quad \dots (20)$$

The projection of the heliostat normal onto this plane is

$$\vec{h}'' = \vec{h} - (\vec{h} \cdot \vec{m})\vec{m} \quad \dots (21)$$

and the yaw angle is

$$\gamma = \cos^{-1} \left( \frac{\vec{T} \cdot \vec{h}''}{|\vec{T} \cdot \vec{h}''|} \right) \quad \dots (22)$$

Finally, the projected width of the heliostat in the  $T$  plane is

$$W' = W \cos \gamma \quad \dots (23)$$

The blocked image is given by (see figure 4)

$$A_{bl} = \sum_{i=2}^4 \max [0, (|W'| - |\Delta W|)] \times \max [0, (|H'| - |\Delta H|)] \quad \dots (24)$$

The absolute values "map" the overlapping images onto the first quadrant. The blocking efficiency is

$$\eta_{bl} = 1 - \frac{A_{bl}}{H'W'} \quad \dots (25)$$

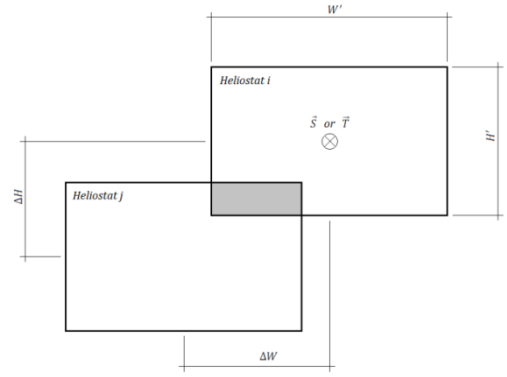


**Figure 4.** Conceptual model for heliostat mapping for shading/blocking.

## 2.4 Shading Efficiency

The same procedure is followed to calculate the shading efficiency. For shading, a stencil of 6 neighbouring heliostats is used, as shown in figure 5, and the tower vector is replaced by the sun vector. Only heliostats in front of the reference heliostat relative to the sun have the potential to cast a shadow onto the reference heliostat.

The power sent to the receiver is found from summation over all zones

$$P = \sum_{i=1}^n \left( \sum_{j=1}^m \eta_{cos} \eta_{bl} \eta_{sh} \eta_{rf} N_{i,j} H \times W \times DNI \right) \quad \dots (26)$$

Fouling, reflection, and attenuation losses are lumped into  $\eta_{rf}$ , which is assumed constant. Results presented in the next section only include the cosine, blocking and shading efficiencies.  $N_{i,j}$  is the number of heliostats in the zone.

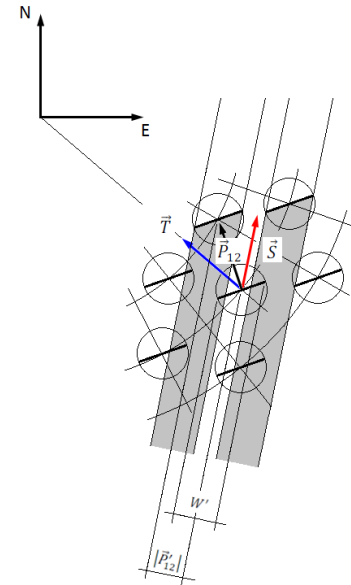


**Figure 5.** Shading stencil for radially staggered field.

### 3. Results

We have assumed a radially staggered surround heliostat field on a perfectly flat and horizontal topography, as shown in figure 1. The staggered approximation is representative of the outer heliostat field of the Gemasolar plant in Spain [13], but not for the inner field. It would appear that a minimum spacing between heliostats in a ring is employed in the inner field. No restriction was placed on the receiver's ability to absorb energy from the heliostat field. Gemasolar was selected as an example since some key parameters [1] and unofficial simulation results of its performance are freely available [17, 18 and, 19]. The distance of heliostats from the tower was obtained from the build-in measurement tool in [13]. Detailed performance data from operating commercial plant would probably not be released in the near future.

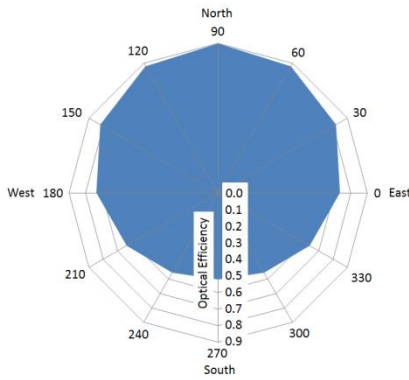


**Figure 6.** Radar plot of field efficiency of representative heliostats 466 m from tower at plant design point (noon, Spring equinox, Northern Hemisphere).

Instantaneous model outputs seem realistic, as shown in figures 6 and 7, also when compared with the detailed results of Ausburger [19]. Hourly model outputs for a full calendar year shows that the overall agreement with Gauche et al [9] is good for small zenith angles, but rather large deviations occurs for zenith angles greater than 70°, as shown in figure 8. This is to be expected, as sunlight will be intercepted by heliostats outside the shading stencil when the sun is low above the horizon. Furthermore, the model of Gauche et al is based upon an in-line heliostat lay-out in a Cartesian grid. Hence, all cells are likely become aligned with the sun direction under certain conditions, leading to a significantly higher shading effect. Leonardi and D'Aguanno [6], analysing a densely packed heliostat field, also found that the optical efficiency tends to zero as  $\theta \rightarrow 90^\circ$ . Their heliostat field has a maximum radius of 140 m, a tower height of 50 m, and a land coverage factor of nearly 58 %.

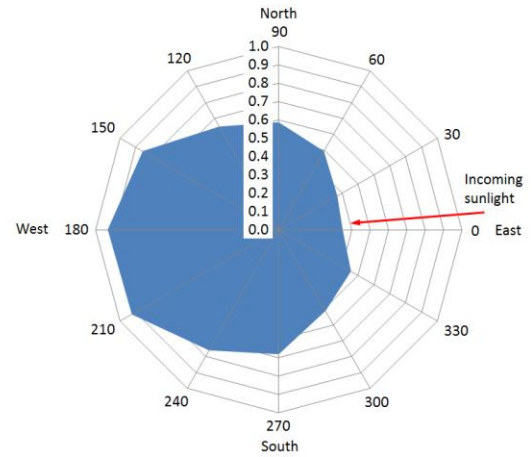


**Figure 7.** Radar plot of shading efficiency of representative heliostats 466 m from tower at 07:00 on Summer solstice (Northern Hemisphere).

For the Gemasolar plant, land coverage is only about 13 %. Their field comprise of staggered heliostats in a Cartesian grid, with heliostats around the edges removed to yield a surround field. Hence, their field is somewhat similar to that analysed by Gauche et al [11]. In a radially staggered lay-out, alignment tends to be more localized at all times. This observation is corroborated by Ausburger [19].

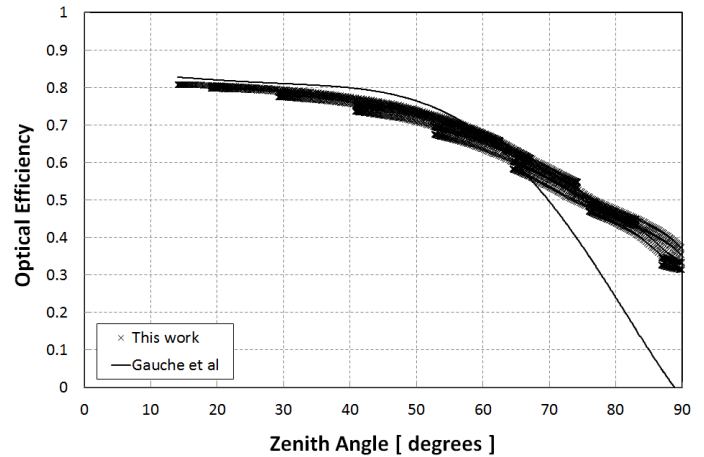


**Figure 8.** Field efficiency as a function of the zenith angle.

However, the main interest is on the energy collected at the receiver, and since

$$DNI \propto e^{-\sec \theta} \quad \dots (27)$$

it means that the DNI drops rapidly with increasing zenith angle as the zenith angle approaches 90° since

$$\lim_{\theta \rightarrow 90^\circ} \sec \theta \rightarrow \infty \quad \dots (28)$$

As the receiver requires a minimum heat flux to prevent solidification of the molten salt, the plant will only start up well after sunrise, and shut down again well before sunset [20]. Hence, correct prediction of the heliostat field optical efficiency at large zenith angles is not that critical. The current model with its rather small stencil for blocking and shading calculations is surprisingly accurate for its intended purpose during normal plant operating hours. Increasing the stencil and additional row towards and away from the tower respectively will triple the number of calculations, with insignificant real returns.

The overall optical efficiency of the field is dominated by the zenith angle, as shown in figure 8. Leonardi and D'Aguzzo [6] and Gauche et al [9] reported similar findings. There is also a secondary effect due to the azimuth angle. Azimuth angle dependence is reported by Leonardi and D'Aguzzo [6]. The data presented in figure 8 is correlated by

$$\eta_{opt} = 0.7769 + 0.1377\theta - 0.1833\theta^2 - 0.05625\theta^3 \quad \dots (29)$$

with a correlation coefficient of 0.985. Insignificant improvement is obtained with a correlation of the form

$$\eta_{opt} = f(\theta)g(\phi) \quad \dots (30)$$

No direct comparison is possible with the work done at the National Renewable Energy Laboratory [17], as they predicted the annual electric energy produced by the plant. Adopting a thermal efficiency of 40 % for the turbine, and realistic values for spillage, convection and radiation losses, the annual electric output is over-predicted by approximately 20 % based upon the total collected energy. This can be partly explained by the fact that here no provision was made for defocussing heliostats if the thermal energy storage should become fully charged during the summer months.

#### 4. Validation

The poor agreement between the current model and that of Gauche et al [9] at large zenith angles prompted further validation of the current model. The shading coefficient predicted by the model for a cell 30° north of east, on a mean radius of 466 m from the tower was validated against a CAD model [21] of one reference heliostat. The reference heliostat was created in the stow position, and then rotated so that its face normal  $\vec{n}$  corresponds to

$$\vec{n} = \frac{\vec{s} + \vec{r}}{|\vec{s} + \vec{r}|} \quad \dots (31)$$

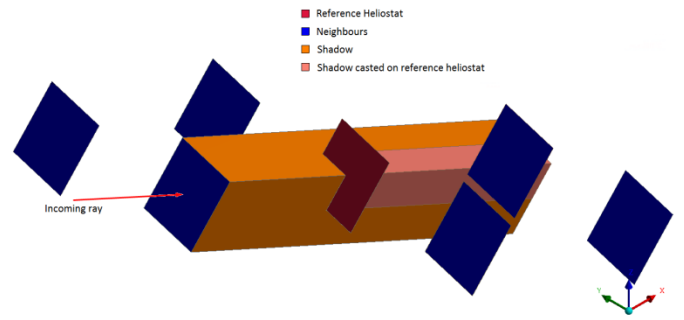


**Figure 9.** Shadow cast by neighbour onto reference heliostat.

The shadows of all six neighbouring heliostats were projected along a ray from the sun, and the intercept of these shadows onto the reference heliostat calculated. A comparison was made for 18:00 on the summer solstice (Northern Hemisphere), as shown in figure 9, a relatively extreme case with the sun low above the horizon. The model predicted a shading efficiency of 0.752, compared to 0.759 predicted by the CAD model. Hence, it is deemed that the model output is correct, and that the deviation from Gauche et al [9] is due to an inadequate shading stencil at large zenith angles, and the dissimilar field lay-outs.

#### 5. Conclusion

A model is presented to calculate the optical (cosine, blocking and shading) efficiency for a radially staggered heliostat field based upon a lumped geometric approach. The annual collected energy is available almost instantaneously (about 2 seconds run-time on an Intel i7 processor with a 32 bit C++ code). The model was validated against data of Gauche et al [9] and Ausburger [16]. It is capable of capturing the main physics of the problem, and the results are accurate enough for macro decision making. It is not capable, or accurate enough for field design and optimization calculations. For these calculations, the performance of each individual heliostat should be considered. The model under predicts the shading effect at large zenith angles. However, the worst performance of this method corresponds with the lowest DNI values, and its impact on plant simulations is expected to be minimal.

#### References

- [1] Anonymous, (s.a.), Torresol Energy, [http://www.torresolenergy.com/EPORTAL\\_DOCS/GENERAL/SENERV2/DOC-cw4cb709fe34477/GEMASOLARPLANT.pdf](http://www.torresolenergy.com/EPORTAL_DOCS/GENERAL/SENERV2/DOC-cw4cb709fe34477/GEMASOLARPLANT.pdf), Accessed 24 October 2014.
- [2] Anonymous, (s.a.), BrightSource Energy, <http://www.ivanpahsolar.com/about>, Accessed 24 October 2014.

- [3] Anonymous, (s.a.), SolarReserve, <http://www.solarreserve.com/what-we-do/csp-projects/crescent-dunes/>, Accessed 24 October 2014.
- [4] Anonymous, (s.a.), Abengoa Solar, [http://www.abengoa.com/web/en/nuestras\\_plantas/plantas\\_en\\_construccion/sudafrica/](http://www.abengoa.com/web/en/nuestras_plantas/plantas_en_construccion/sudafrica/), Accessed 24 October 2014.
- [5] P. Schwarzbözl, M. Schmitz, M. and R. Pitz-Paal, (2009). Visual HFCAL – A Software for Layout and Optimization of Heliostat Fields, SolarPACES 2009, Berlin.
- [6] E. Leonardi and B. D’Aguanno, CRS4-2: A Numerical Code for Calculation of the Solar Power Collected in a Central Receiver System, *Energy*, 36 (2011) 4828 – 4837.
- [7] F.J. Collado and J. Guallar, Campo: Generation of Regular Heliostat Fields, *Renewable Energy*, 46 (2012) 49 – 59.
- [8] S.L. Lutchman et al, On Using a Gradient-based Method for Heliostat Field Layout Optimization, *Energy Procedia*, 49 (2014) 1429 – 1438.
- [9] P. Gauche et al, (2012). Modeling Dispatchability Potential of CSP in South Africa, SASEC 2009, Stellenbosch.
- [10] R.A.Haman, D.K. Aldweni and M.A. Elayeb, M.A., (2013). Study of Optical Losses in Heliostat Fields, Proceedings of the 4<sup>th</sup> DII Desert Energy Conference, Rabat.
- [11] P. Gauche, T.W. Von Backström and A.C. Brent, (2011). CSP Modeling Methodology for Macro Decision Making – Emphasis on the Central Receiver Type, SolarPACES 2011, Granada.
- [12] J.A. Duffie and W.A. Beckman, (2006). *Solar Engineering of Thermal Processes*, 3<sup>rd</sup> Edition, John Wiley & Sons, Hoboken, New Jersey.
- [13] Anonymous, (2014), Google Maps, available at <https://www.google.co.za/maps/place/GEMASOLAR/@37.561078,5.331545,12z/data=!4m2!3m1!1s0x0:0x1527431768917882>, Accessed 23 October 2014.
- [14] G. Sassi, Some Notes on Shadow and Blockage Effects, *Solar Energy*, 31 (1982) 331 - 333.
- [15] F.M.F. Siala, and M.E. Elayeb, Mathematical Formulation of a Graphical Method for a No-Blocking Heliostat Field Layout, *Renewable Energy*, 23, (2001) 77 – 92.
- [16] Anonymous, (s.a.), <http://mathworld.wolfram.com/Projection.html>, Accessed 24 October 2014.
- [17] Anonymous, (s.a.), System Advisor Model (SAM) Case Study: Gemasolar, NREL Report, available at [https://sam.nrel.gov/sites/sam.nrel.gov/files/content/case\\_studies/sam\\_case\\_csp\\_salt\\_tower\\_gemasolar\\_2013-1-15.pdf](https://sam.nrel.gov/sites/sam.nrel.gov/files/content/case_studies/sam_case_csp_salt_tower_gemasolar_2013-1-15.pdf)
- [18] Anonymous, (s.a.), National Renewable Energy Laboratory: System Advisor Model, available at <https://sam.nrel.gov>, Accessed 24 October 2014.
- [19] G. Augsburger, (2013). Thermo-economic Optimisation of Large Solar Tower Power Plants, Ph D Thesis, Swiss Federal Institute of Technology, Lausanne.
- [20] J. I. Burgaleta et al, (2012). Gemasolar, Key Points for the Operation of the Plant, SolarPACES 2012, Marrakesh.
- [21] Anonymous, (s.a.), <http://www.ansys.com/Products/Workflow+Technology/ANSYS+Workbench+Platform/ANSYS+DesignModeler>, Accessed 24 October 2014.